Above-threshold ionization of negative hydrogen

L. A. A. Nikolopoulos and P. Lambropoulos
Department of Physics, University of Crete and Institute of Electronic Structure and Laser, Heraklion-Crete 71110, Greece and Max-Planck-Institut für Quantenoptik, Garching 85748, Germany
(Received 23 May 1997)

We present detailed calculations for two-and three-photon above-threshold ionization of the negative hydrogen ion. In addition to calculated values for partial wave amplitudes and phase shifts pertaining to recent experimental results [Xin Miao Zhao *et al.*, Phys. Rev. Lett. **78**, 1656 (1997)], we also address the question of the asymmetry of photoelectron angular distributions in ionization under elliptically polarized radiation, which has been studied experimentally in other negative ions [C. Blondel and C. Delsart, Laser Phys. **3**, 3 (1993); Nucl. Instrum. Methods Phys. Res. B **79**, 156 (1993); F. Dulieu, C. Blondel, and C. Delsart, J. Phys. B **28**, 3861 (1995)]. [S1050-2947(97)08810-0]

PACS number(s): 32.80.Wr, 32.80.Rm, 32.80.Gc

I. INTRODUCTION

It has been known [1–7] for quite some time now that multiphoton ionization of atoms with radiation elliptically polarized can lead to photoelectron angular distributions (PAD) lacking the usual fourfold symmetry found under linearly or circularly polarized radiation. This effect is present in the fundamental description of the process in perturbation theory and has been indentified to be connected to the nonzero value of the phase shift of the final continuum state. Formally the phase shift leads to a complex multiphoton transition amplitude, which when combined with the ellipticity parameter produces terms that, depending on the values of the other parameters (such as radial matrix elements), can lead in general to a more or less asymmetric PAD. From the structure of the resulting expressions it is evident that if the phase shifts of all partial waves were zero (corresponding to plane waves) the asymmetry would disappear. The continuum state resulting from electron detachment of a negative ion might be thought of as coming as close to a plane wave as one can expect in a real system with a bound initial state. This aspect has been investigated experimentally by Blondel and collaborators, who have produced extensive results on PAD's including elliptical polarization, which has not shown any significant asymmetry. Is it because of a near plane wave character of the final state?

Above-threshold ionization (ATI) adds a further aspect to this question. A multiphoton transition amplitude involving absorptions within the continuum, as ATI does, is by necessity complex because of the presence of poles within the continuum. This led one of us (P.L.), some time ago, to the assertion that the asymmetry should be present in ATI even if all phase shifts were zero, which has to be understood as the limit to plane waves. As we shall see later on, that assertion was overenthusiastic and the actual situation is subtler. It was nevertheless that question in fact that motivated Blondel and collaborators to search for that asymmetry in negative ions including ATI in one case. It is against this background that we undertook the present work in negative hydrogen.

Our chief objective was to explore in a quantitative setting the question of the asymmetry including ATI. Negative hydrogen being a two-electron system poses serious demands on the calculations of multiphoton transitions as illustrated by previous work [8–15] on aspects of this system. Our approach has evolved as a side product of our work on the nonpertubative solution of the time-dependent Schrödinger equation for two-electron atoms in strong laser fields [16–19], with the atomic structure handled in terms of L^2 discretized bases constructed as linear combinations of B splines [20,21]. The calculation of ATI through a discretized basis also requires appropriate handling, as discussed elsewhere [22], where a new versatile method applicable to any discretized basis has been shown to provide accurate results within perturbation theory, which is the case of interest here. Through a combination of the above techniques, we have been in a position to obtain results on two- and three-photon ionization including ATI over an extensive energy range, which by a happy coincidence also covers the range of experimental data reported most recently by Zhao *et al.* [1]. We have at the same time examined PAD's for polarization of varying degree of ellipticity and, as discussed in the following sections, the asymmetry is in general present depending of course on the degree of ellipticity and the wavelength of the radiation, as expected to be the case. One of the chief advantages of and motivation for studies in negative hydrogen is its fundamental significance as a negative ion and at the same time a very special two-electron system combined with the possibility of performing accurate *ab initio* calculations. Atomic units are used throughout this work.

II. THEORY

A. Photoelectron angular distributions

The transition probability per unit time within lowest nonvanishing order of pertubation theory for nonresonant N-photon ionization can be written as

$$W_{fg}^{(N)} = \hat{\sigma}_N I^N, \tag{1}$$

where $\hat{\sigma}_N$ is the total angle-integrated generalized cross section given by

$$\hat{\sigma}_N = \frac{(2\pi\alpha)^N k}{4\pi^2}\,\omega_L^N \int d\Omega_{\mathbf{k}} |M_{fg}^{(N)}|^2, \tag{2}$$

with α being the fine structure constant, $\mathbf{k}$ the wave vector of the outgoing photoelectron related to its energy by $E_k = k^2/2$, the integration is over all angles of propagation of the photoelectron and the symbols f,g denote the final and initial state, respectively.

The dependence of the angular distribution of the photoelectrons on the atomic structure and the polarization $\hat{\mathbf{e}}$ of the field is now contained in the quantity $M_{fg}^{(N)}$ defined by

$$M_{fg}^{(N)} = \sum_{\nu_{N-1}} \cdots \sum_{\nu_1} \frac{\langle f|\mathbf{D}\hat{\mathbf{e}}|\nu_{N-1}\rangle \cdots \langle \nu_1|\mathbf{D}\hat{\mathbf{e}}|g\rangle}{[\omega_g + (N-1)\omega_L - \omega_{\nu_{N-1}}]\cdots[\omega_g - \omega_{\nu_1} + \omega_L]}, \tag{3}$$

where $\mathbf{D}$ is the atomic dipole moment operator that can be expressed either in the length ($\mathbf{D} = q\mathbf{r}$) or in the velocity gauge ($\mathbf{D} = q\boldsymbol{\nabla}/\omega_L$), with q being the electronic charge. The summations are carried out over all possible intermediate states including the discrete and continuous parts of the atomic spectrum. The generalization of Eq. (3) to ATI of order $N+R$, where N photons are needed to ionize the atom plus R extra photons, which are absorbed in the continuum, involves the presence of poles in the integral. In that case, Eq. (3) requires the removal of the poles from the real axis through quantities ϵ_i and taking their limits to zero [23].

Although spin-orbit coupling plays no role in this work, we have chosen, for the sake of completeness of the formalism, to exhibit the spin variable m_s in the final state of the photoelectron and the core. Alternatively, we could have written all equations without reference to spin. In general, in order to calculate the photoelectron angular distribution for a process that leaves the residual core in a state characterized by l_c, m_c, and m_{s_c} quantum numbers, the continuum states are expanded as

$$|f_{l_c,m_c,m_{s_c}};\hat{\mathbf{k}},m_s\rangle = \sum_{J_f,l,m} i^l e^{-i\delta_l} Y_{lm}^{\star}(\hat{\mathbf{k}})(SLJ_fM_{J_F}|SM_SLM_L) \times (s_csSM_S|s_cm_{s_c}sm_s)(l_clLM_L|l_cm_clm)|SLJ_fM_{J_f}\rangle, \tag{4}$$

where J_f are the allowed angular momenta and l,m,m_s the associated partial waves for the outgoing photoelectron. The explicit presence of the core states, as we already discussed, is here important only when one wants to calculate photoelectron angular distributions. The angles in the spherical harmonic specify the direction of propagation $\mathbf{k}$ of the photoelectron. These angles are in reference to a Cartesian system of coordinates whose z axis is taken along $\hat{\mathbf{e}}$ for linearly polarized light and along the photon propagation vector for elliptically or circularly polarized light. In the present case, the polarization vector is written as $\hat{\mathbf{e}} = (1+\eta^2)^{-1/2}(\hat{\mathbf{x}} + i\eta\hat{\mathbf{y}})$ where the ellipticity parameter η varies from 1 to -1.

Substituting the above state representation into Eq. (3) and carrying out the angular momentum algebra we obtain [12]:

$$M^{(N)}(l_c,m_c,m_{s_c};\hat{\mathbf{k}},m_s;\eta) = \sum_{J_f,l,m} i^l e^{-i\delta_l}(-1)^{L-S+l-l_c-M_{J_f}-M_S-M_L} Y_{lm}^{\star}(\hat{\mathbf{k}}) D_{J_f}^{(N)}(\eta)[(2J_f+1)(2L+1)(2S+1)]^{1/2} \times \begin{pmatrix} S & L & J_f \\ M_S & M_L & -M_f \end{pmatrix} \begin{pmatrix} s_c & s & S \\ m_{s_c} & m_s & -M_S \end{pmatrix} \begin{pmatrix} l_c & l & L \\ m_c & m_e & -M_L \end{pmatrix}. \tag{5}$$

Here $D_{J_f}^{(N)}$ is given in Eq. (3) with the difference that the final state is of the form $|SLJ_fM_{J_f}\rangle$:

$$D_{J_f}^{(N)} \equiv \sum_{\nu_{N-1}} \cdots \sum_{\nu_1} \frac{\langle SLJ_fM_{J_f}|\mathbf{D}\hat{\mathbf{e}}|\nu_{N-1}\rangle \cdots \langle \nu_1|\mathbf{D}\hat{\mathbf{e}}|g\rangle}{[\omega_g + (N-1)\omega_L - \omega_{\nu_{N-1}}]\cdots[\omega_g - \omega_{\nu_1} - \omega_L]}. \tag{6}$$

The differential cross section for N-photon ionization is given by

$$\frac{d\hat{\sigma}_N(l_c;\hat{\mathbf{k}};\eta)}{d\Omega} = 2\pi(2\pi\alpha)^N \sum_{m_c,m_{s_c},m_s} |M^{(N)}(l_c,m_c,m_{s_c};\hat{\mathbf{k}},m_s;\eta)|^2 \tag{7}$$

from which integrating over all angles we obtain the N-photon generalized cross section as

$$\hat{\sigma}_N = 2\pi(2\pi\alpha)^N \sum_{J_f} |D_{J_f}^{(N)}(\eta)|^2. \quad (8)$$

The exact dependence on the photoelectron angles and the ellipticity η of the quantity $M_{fg}^{(N)}$, for $N=2,3$, are given in Appendix A. Given the initial and final ion state, Eq. (5) contains all the necessary information to calculate angular distributions since $|M^{(N)}|^2$ is proportional to $d\hat{\sigma}_N/d\Omega$. The unknown quantities are the $D_{J_f}^{(N)}$ for each ionization channel. The way in which we calculate these quantities is described in the next section.

B. Atomic basis

The computational procedure used here has been presented in detail in a series of articles [11,24,25]. In brief, we use one-electron hydrogenic orbitals:

$$\phi_{nlmm_s}(\mathbf{r}) = \frac{\chi_{nl}(r)}{r} Y_{lm}(\theta,\phi)\sigma(m_s). \quad (9)$$

The radial functions $\chi_{nl}(r)$ satisfy the equation:

$$\left(-\frac{1}{2}\frac{d^2}{dr^2} - \frac{Z}{r} + \frac{1}{2}\frac{l(l+1)}{r^2}\right)\chi_{nl}(r) = E_{nl}\chi_{nl}(r), \quad (10)$$

with E_{nl} being the eigenvalue. The χ_{nl} functions with negative or positive eigenvalues are expanded on a set of B splines of order k and total number p defined in the finite interval $[0,R_{\max}]$. Two-electron states with total angular momentum L are constructed in the LS coupling of two-electron configuration space $\Psi_{n_j l_1, n_2 l_2}^{SL}(\mathbf{r}_1,\mathbf{r}_2) = A|l_1 s_1 l_2 s_2 LMSM_s\rangle R_{n_1 l_1, n_2 l_2}(r_1,r_2)$ where A represents the antisymmetrization operator. The two-electron energy eigenfunctions are written in the form [26]

$$\Phi_{n(E)}^{SL} = \sum_{n_1 l_1, n_2 l_2} C_{n(E)}^{SL}(n_1 l_1, n_2 l_2)\Psi_{n_1 l_1, n_2 l_2}^{SL}(\mathbf{r}_1,\mathbf{r}_2), \quad (11)$$

where $C_{n(E)}^{SL}(n_1 l_1, n_2 l_2)$ is the eigenvector of the atomic Hamiltonian matrix for the nth energy eigenvalue. Here $|C_{n(E)}^{SL}(n_1 l_1, n_2 l_2)|^2$ is the probability density for the configuration $(n_1 l_1, n_2 e_2)$ in the nth energy eigenstate. For $E>0$, $\Phi_{n(E)}^{SL}$ represents discretized continuum states. In the present case, the order of B splines is $k=9$ with $p=150$ and $R_{\max}=150$ a.u. The knot sequence that we use is sinelike used first by Tang and Chang [11] for calculations of multiphoton processes. In that reference, one can find the details of the method we have used to calculate the phase shifts for each channel $L=0,1,2,3$ needed for the PAD's.

In order to calculate the summations over intermediate states in the ATI case, we use the recently developed extrapolation method whose details can be found in [22]. Because of the discretization of the continuum, the detachment rates and phase shifts are calculated for discrete energies.

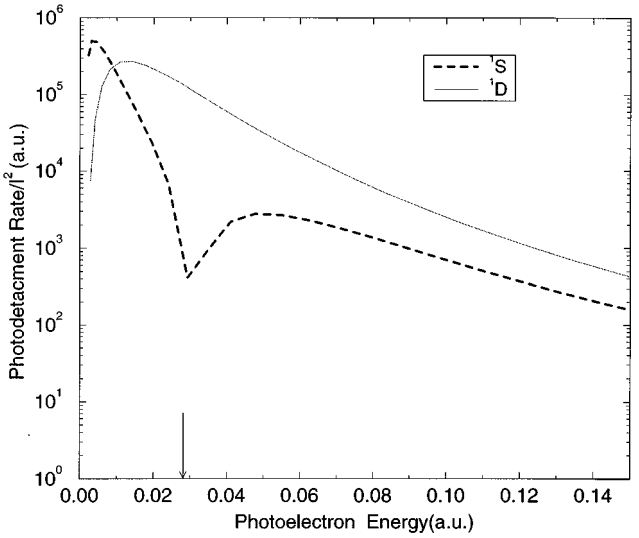

FIG. 1. Photodetachment partial rates in a.u. for two-photon ionization. Energy region covers ionization with and without ATI, which begins at photoelectron energy 0.0277 a.u. (indicated by the arrow). Note that 1 a.u. of energy is 27.112 eV, while 1 a.u. of rate is 2.41×10^{-17} s^{-1}.

Consequently, these rates and phase shifts in general do not coincide for different channels. For the energy region that we examine, the smoothness and density of data points are sufficient to use a cybic spline interpolation in order to obtain data for intermediate energies. The value of the ground state differs by about 14% from that calculated by Pekeris [27]. To obtain a better ground-state energy, we would have to include a large number of states within each series of configurations associated with each excited ''inner'' electron. Calculations of ATI by a discretized basis require a sufficiently dense spacing of continuum states, which must also extend high in energy. In order to have continuum wave functions, as well as the correlated ground state simultaneously, our primary criterion was the agreement between velocity and length gauge for the calculated dipole matrix elements. With much more effort, the ground-state energy could be improved, but would not have a significant effect on the quantities of interest in this work.

III. RESULTS

A. Two-photon detachment

We consider absorption of two photons from the ground state of negative hydrogen in the photoelectron energy region (0–0.15 a.u.). From the dipole selection rules, the number of independent channels are two, with final total angular momenta $L=0,2$ (i.e., S and D). The resulting H atom for these energies remains in its ground state and so we also have $J_f=0,2$. In Fig. 1, we show, for linearly polarized light, the partial photodetachment rates $\Gamma(S)$ and $\Gamma(D)$ where Γ is the intensity-independent rate in a.u. defined by

$$\frac{1}{I^2}\Gamma^{(2)}(i) = 2\pi(2\pi\alpha)^2 |D_i^{(2)}(\eta=0)|^2, \quad i=S,D. \quad (12)$$

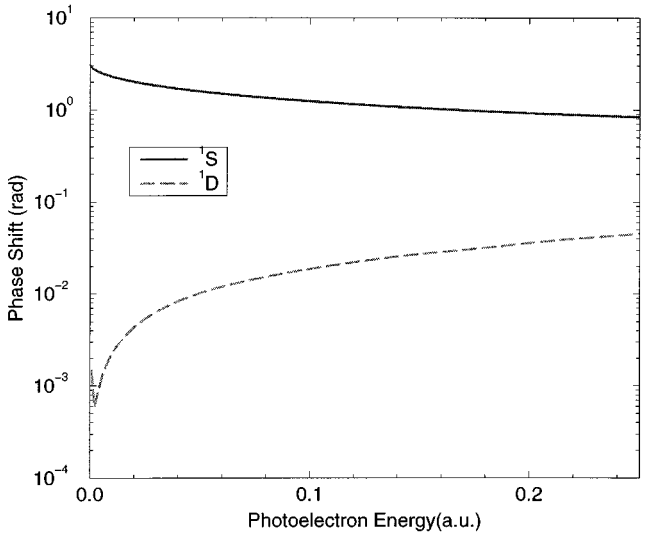

FIG. 2. Phase shifts corresponding to channels S and D with angular momentum $L=0,2$.

Our calculations are in good agreement with those of van der Hart [15] in the case without ATI. The same holds true for the calculations that Proulx and Shakeshaft [8,9] have performed for two-photon ionization for a wide photon energy region. Calculations of cross sections for two-photon above-threshold detachment of negative hydrogen have also been performed by Sanchez *et al.* [13] for a different photon energy region. Very recently, in experimental work [1] in negative hydrogen with ATI at photoelectron energy about 0.058 a.u. the brancing ratio of the S and D partial waves has been measured. For this particular energy, the reported data show branching by $90\% \pm 10\%$ into the D wave, an observation that is in excellent agreement with our calculations, which predict 89%. Furthermore, the agreement between our theoretical values and the experimental ones suggests that for laser intensities at least up to 3×10^{10} W/cm^2 the interaction between the negative hydrogen and the laser field can be described well by pertubation theory.

Turning now to our results, we see that the dominant contribution comes from the D symmetry. We also note the threshold behavior where the dominant channel is the channel with the lowest angular momentum, an effect well established for negative ions from the Wigner law:

$$\sigma_l \sim \epsilon^{l+1/2}. \tag{13}$$

This particular behavior for negative ions originates from the absence of a long-range Coulomb potential for the outgoing photoelectron. Also we note that a rise in the detachment rate for the partial wave, which corresponds to the lowest angular momentum, occurs when the photoelectron reaches an energy of about 0.028 a.u. The agreement between length and velocity gauge remains satisfactory throughout the energy region under consideration. The difference is within the thickness of the line of the graphs. The phase shifts for the channels $L=0,2$ necessary for the calculation of PAD are shown in Fig. 2. From that figure, it is evident that since the phase shift of the channel S is considerably different from zero, it exhibits a strong nonplane wave

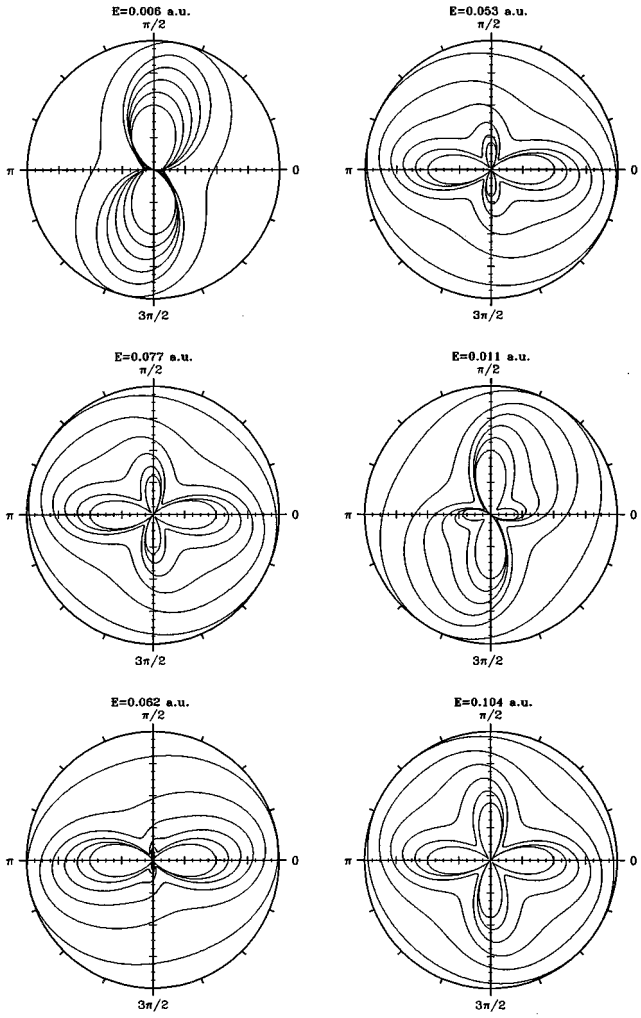

FIG. 3. Two-photon detachment angular distributions as functions of ϕ of photoelectrons for kinetic energies $E_p=0.006$, 0.0583, 0.077, 0.011, 0.062, 0.104 a.u. and for various values of the ellipticity parameter (starting from the inner graphs) $\eta=0.0$, 0.18, 0.36, 0.54, 0.70, 0.90. For visual facility, the azimuthal angular dependence distribution is on the polarization plane ($\theta_k=\pi/2$) and the polar plots have been expanded with increasing ellipticity. This does not imply increasing rate with ellipticity.

behavior for a rather large photoelectron energy range. As expected, the value of the phase shift decreases with the energy of the outgoing electron. Using Eq. (5), after the interpolation in energies and phase shifts for the channels S,D, we produce angular distributions for different photon energies and various values of the ellipticity parameter η (Fig. 3). These graphs reveal a gradually increasing asymmetry on angle θ, as the absolute value of the ellipticity parameter increases. The value $\eta=0$ corresponds to linear polarization where it is well established that the angular distributions have fourfold symmetry. The asymmetry can in principle always be present for elliptical polarization, independently of whether we have excess photon absorption or not. A brief argument as to why that happens is the following. The structure of the angular dependence of the outgoing photoelectron in the case of elliptical polarization for a fixed θ and for arbitrary number of absorbed photons will be of the type [7]

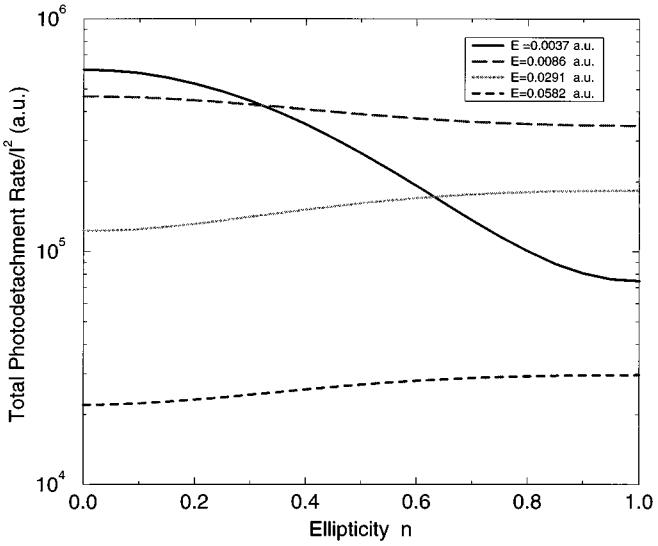

FIG. 4. Total two-photon detachment rate as a function of the ellipticity η of the light for four photoelectron energies. Photoelectron energies correspond to ATI and no-ATI cases.

$$M_{fg}^{(N+R)}=\left|\sum_m a_m e^{im\phi}\right|^2, \tag{14}$$

where all the nonvanishing terms have either even or odd m. The amplitudes a_m are integrals over the intermediate states involving the reduced radial elements. From the above formula, we are led to fourfold symmetry when the amplitudes are real. The amplitudes in a multiphoton process are complex for two reasons [6]. The first reason is that, in the continuum, in the absence of spin, which for this argument is unimportant, the wave functions of photoelectrons can be written as [28]

$$|\mathbf{k}\rangle=4\pi\sum_{t=0}^{\infty}\sum_{m_l=-l}^{l} i^l e^{-i\delta_l} G_{kl}(k,r) Y_{lm_l}(\theta\phi) Y^*_{lm_l}(\theta_k\phi_k), \tag{15}$$

where δ_l are the phase shifts due to the potential of the atom and $G_{kl}(k,r)$ are real radial functions. Therefore the complex amplitude here is due to the existence of phase shifts. The second reason has to do with the case in which we have an excess photon absorption (ATI). The presence of the poles at certain energies in the integrals α_m introduces an imaginary part at these energies. Thus even when we have no ATI, in the elliptical case, the asymmetry in angular distributions can appear because of the phase shifts. In the present case, the existence of the asymmetry when we do not have ATI suggests that the state of the outgoing photoelectron is not a plane wave. Now regarding the ATI case, it can be proven (see Appendix B) that in the perturbation theory regime and the plane wave approximation, under the assumption that there are no other bound states except the ground one, the fourfold symmetry is conserved. A different argument by Crance [29], assuming plane waves for the photoelectron, leads to the same conclusion. Finally we present the total detachment rate (Fig. 4) as a function of the ellipticity η of the light for selected photoelectron energies. The explicit form for the detachment rate is given in Appendix A. From this graph it is apparent that when the dominant partial wave corresponds to the lower angular momentum (here the S wave) there is a large decrease for the transition rate with increasing ellipticity of the light, i.e., going from linear toward circular. That is what is expected in general, since the number of possible paths that end up to the final state, for a multiphoton process, is the maximum one when the light is linearly polarized. But when the dominant partial wave corresponds to higher angular momentum (here the D wave) it is possible to observe a different behavior for the transition rate, namely, its increase with increasing ellipticity of the light. But there is an upper limit for this increase $\Gamma(\eta=1)/\Gamma(\eta=0)\rightarrow 1.5$ when $A_S/A_D\rightarrow 0$, as is known [30], which is easily obtained if one considers the two limiting cases $\eta=0$ (linear light) and $\eta=1$ (circular light) in the corresponding formulas in Appendix A, where the definition of symbols A_S, A_D can be found.

B. Three-photon detachment

Here we calculate partial photodetachment rates and angular distributions for elliptically polarized light, for the case of three-photon ionization in the energy region where it is possible to have one and two excess photon absorptions. Now the angular momentum of the final states can be $L=1,3$ and again we consider the case where the resulting H atom remains in its ground state. The order of the process now is higher than for the two-photon case and we need to enlarge the atomic basis in order to preserve the reliability of the calculations. The reason for this is that the extrapolation method [22] we use demands a sufficiently high density of states in the energy region where the poles occur. The suitable density of states depends also on the photon energy, independently of the order of the process. Consequently we enlarge the box radius to 250 a.u. and at the same time we improve the quality of the B-spline set, taking $k=11$, $p=202$, and a knot sequence that is dense in the energy region close to the nucleus and that decreases nearly linearly far away from the nucleus. The value of the ground state that we obtain differs from that of Pekeris as much as in the two-photon case. In Fig. 5, we show partial photodetachment rates for the symmetries $L=1,3$. Again the dominant contribution to the detachment rate near the threshold comes from the partial wave with the lower angular momentum as expected from Wigner's law.

At this point, it is perhaps useful to discuss a feature of N-photon detachment, namely, the rise of the rate at every photoelectron energy where a threshold is crossed. This is a general effect that should happen for all negative ions in the ATI case, at energies that can be determined given the electron affinity, the order of the process, and the number of the excess photons. The number of such rises is exactly N, the order of the overall process. The reason for this is again the Wigner threshold law and occurs every time the number of excess photons in ATI increases. The rise is present for each channel, but the Wigner law leads to a sharper rise for the channel with the lowest angular momentum. If the electron affinity is E_{af}, the order of the process N, and the number of

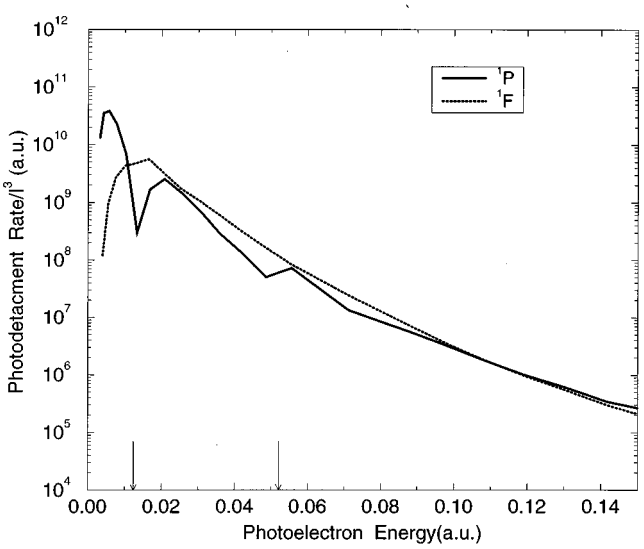

FIG. 5. Photodetachment partial rates in a.u. for three-photon ionization. Energy region covers ionization with and without ATI, which begins at 0.0139 a.u. (arrow) while the ATI involving two photons begins at 0.0554 a.u. (second arrow).

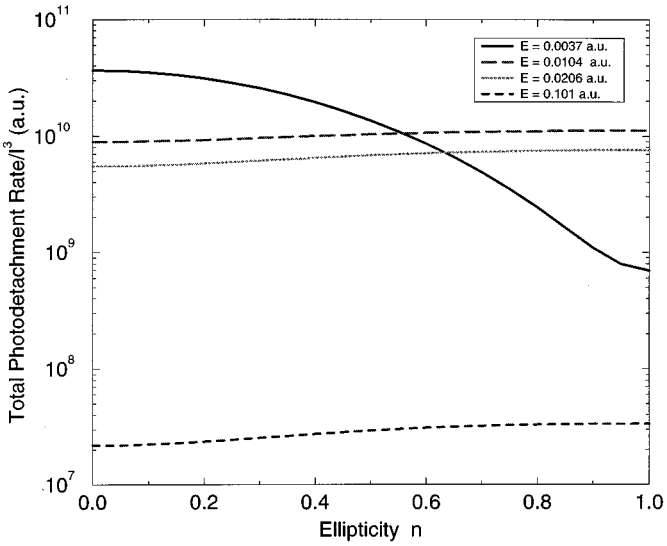

FIG. 6. Total three-photon detachment rate as a function of the ellipticity η of the light for four photoelectron energies. Photoelectron energies correspond to ATI and no-ATI cases.

the excess photons R, then the photoelectron energies E_r at which one should expect rises for the detachment rates (if there is no other reason for this, such as autoionizing states) are given by the formula

$$E_r^{(R)} = E_{\rm af}\frac{R}{N-R}, \quad R = 0,1,2,...,N-1. \tag{16}$$

Therefore, for the two- and three-photon detachment rates and for the energy region that we consider, since there is no structured contunuum, the rises occur at the expected energies and they are completely predictable as we can see from the corresponding figures (Figs. 1 and 5).

$$E_r^{(0)} = 0, \quad E_r^{(1)} = E_{\rm af}, \quad N = 2, \tag{17}$$

$$E_r^{(0)} = 0, \quad E_r^{(1)} = E_{\rm af}/2, \quad E_r^{(2)} = 2E_{\rm af}, \quad N = 3. \tag{18}$$

Now, regarding how large these rises are for a given photoelectron energy, it depends on the number of the excess photons needed to reach this energy. Increasing this number, we should expect a tendency for the rises to be less sharp, since the order of the process is increased.

The above analysis is compatible with the observation of Proulx and Shakeshaft [9] in their investigation of the two- and three-photon detachment rates of negative hydrogen. In the case of three-photon detachment, they found a rise of the detachment rate due completely to a rise in the partial wave corresponding to the lowest angular momentum $L=1$ at a photoelectron energy where the two-photon detachment threshold is located, but not in the two-photon case. That is correct if one examines the total two- or three-photon rates, as Proulx and Shakeshaft did. Since the $L=2$ wave in the two-photon case overwhelms the $L=0$ (see Fig. 1), the rise is masked in the total two-photon rate. On the contrary the $L=1$ and $L=3$ contributions at the position of the rise are comparable in the three-photon case (see Fig. 5), which makes the rise discernible even when the total rate is examined. We have chosen to emphasize the partial wave features, since these threshold effects are intimately connected with the angular momentum. Also, we present total detachment rates (Fig. 6) as a function of the ellipticity of the light. Behavior similar to that of the two-photon case is observed for the three-photon transition rate for selected photoelectron energies. Finally, we present the phase shifts for the channels corresponding to angular momentum $L=1,3$ (Fig. 7). Angular distributions for different energies and various ellipticities are shown in Fig. 8. Here again the asymmetry is observable and increases gradually with increasing ellipticity of the light. Note also the energies of the photoelectrons corresponding to ATI with one ($E_p=0.01018$, 0.0532 a.u.) and two excess ($E_p=0.0617$ a.u.) photons.

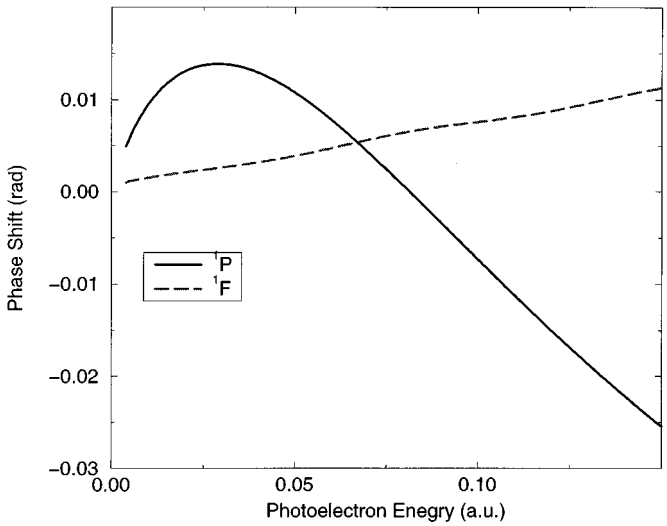

FIG. 7. Phase shifts corresponding to channels P and F with angular momentum $L=1,3$.

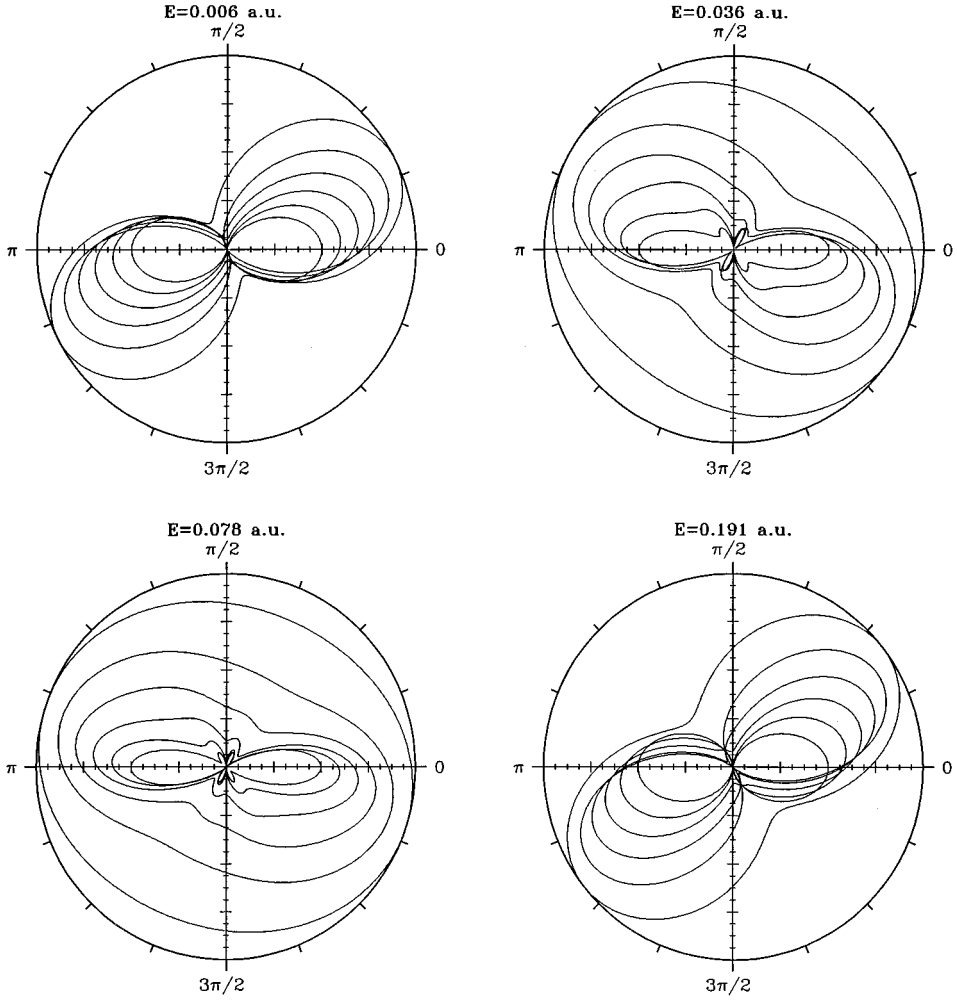

FIG. 8. Three-photon detachment angular distributions as functions of ϕ of photoelectrons for kinetic energies $E_p = 0.006$, 0.036, 0.078, 0.191 a.u. and for various values of the ellipticity parameter as in the two-photon case. For visual facility, the azimuthal angular dependence distribution is on the polarization plane ($\theta_k = \pi/2$) and the polar plots have been expanded with increasing ellipticity. This does not imply increasing rate with ellipticity.

IV. CONCLUSION

As far as the photoelectron angular distributions are concerned, we have shown that elliptical polarization will in principle lead to the breakdown of the fourfold symmetry as is the case with neutral atoms. Of course the degree of asymmetry will depend on the ellipticity parameter as well as the wavelength, and the absence of the asymmetry at some wavelength does not imply its nonexistence. Although our results have been obtained for a case of an S_0 initial state leading to an S_0 residual core, the effect should, if anything, be even more pronounced in more general cases. We have in addition shown that, in the case of a single bound state, the absence of nonzero phase shifts in the continuum states(plane waves) preserves the fourfold asymmetry even in the presence of ATI. This modifies the validity of an assertion made by one of us (P.L.) in an earlier paper [6]. Finally we have provided results for phase shifts and rates into the channels of final states that are in excellent agreement with recent experimental data [1], as well as for the results for three-photon detachment, which may be of use in extensions of the relevant ATI experiments. This work at the same time served as an example of the versatility of the techniques we have employed, which can be readily extended to provide answers even in the nonpertubative regime, when related experimental data become available, as has been shown in the case of two-electron atoms [16–18].

ACKNOWLEDGMENTS

The authors would like to thank Dr. Jian Zhang for much helpful advice regarding the atomic structure of negative hydrogen. One of us (L.N.) would like to also thank P. Maragakis for many valuable discussions on aspects of two-electron atom calculations. Pertinent and useful comments by Dr. C. Blondel on an initial draft of the manuscript are gratefully acknowledged.

APPENDIX A: TWO- AND THREE-PHOTON TRANSITION RATES

Here we present the explicit dependence on the ellipticity of the light of the two- and three-photon total transition rates. The following formulas apply to ionization or detachment

from an atomic system having angular momentum $L=0$ in its ground state. For a two-photon transition the amplitude given by Eq. (5) is

$$M^{(2)}(\eta)=\frac{\sqrt{\pi}}{3(1+\eta^2)}(1-\eta^2)(2A_s-A_D)$$
$$+3A_D[(1-\eta^2)\cos^2\theta_k-(1+\eta^2)$$
$$\times\sin^2\theta_k\cos2\phi_k-i2n\ \sin^2\theta_k\sin 2\phi_k]\},$$
(A1)

where the quantities A_S, A_D are complex in general and given by

$$A_i\equiv\sum_\nu \frac{R^{\nu,P}_{1,S}R^{k,i}_{\nu,P}}{\omega_g-\omega_{\nu P}-\omega_L},\quad i=S,D. \tag{A2}$$

The R's are reduced matrix elements [31] and the subscript i refers to the final value of the angular momentum for each channel. Here the intermediate states, denoted by ν, should be understood as belonging to the discrete and continuum spectrum of symmetry P. The relation between ellipticity η and the polarization vector of the field has already been defined in the main text. The angular variables (θ_k,ϕ_k) determine the direction of the photoelectron in the final state. Integrating the quantity $|M^{(2)}(\eta)|^2$ over these angles, we obtain the total cross section through Eqs. (1) and (2):

$$\frac{1}{2\pi(2\pi\alpha I)^2}W^{(2)}(\eta)=\frac{16\pi^2}{45}\left[5\left(\frac{1-\eta^2}{1+\eta^2}\right)^2|A_S|^2\right.$$
$$\left.+4\frac{1+4\eta^2+\eta^4}{(1+\eta^2)^2}|A_D|^2\right].$$
(A3)

For the three-photon transition, the amplitude is

$$M^{(3)}(\eta)=-i\frac{2\sqrt{\pi}}{(1+\eta^2)^{3/2}}\sin\theta_k$$
$$\times\left[(1-\eta^2)\left(Q_P+\frac{3Q_F}{5}(5\cos^2\theta_k-1)\right)\right.$$
$$\times(\cos\phi_k+i\eta\ \sin\phi_k)-Q_F\sin^2\theta_k[(1+3\eta^2)$$
$$\left.\times\cos3\phi_k+i\eta(3+\eta^2)\sin3\phi_k]\right],$$
(A4)

with Q_P, Q_F:

$$Q_P=\frac{5A_{SP}+4A_{DP}}{15},\quad Q_F=\frac{A_{DF}}{4}$$
(A5)

and A_{SP}, A_{DP}, A_{DF} defined through integrals of reduced matrix elements over discrete and continuum states:

$$A_{L_1,L_2}\equiv\sum_{\nu_1}\sum_{\nu_2}\frac{R^{\nu_1,P}_{1,S}R^{\nu_2,L_1}_{\nu_1,P}R^{k,L_2}_{\nu_2,L_1}}{(\omega_g-\omega_{\nu_1P}-\omega_L)(\omega_g-\omega_{\nu_2L_1}-2\omega_L)},$$
$$L_1=S,D\quad\text{and}\quad L_2=P,F. \tag{A6}$$

From the quantity $|M^{(3)}(\eta)|^2$, performing the integral over the angles, we obtain for the total three-photon transition rate:

$$\frac{1}{2\pi(2\pi\alpha I)^3}W^{(3)}(\eta)=\frac{16\pi^2}{525}\left[\frac{7}{9}\left(\frac{1-\eta^2}{1+\eta^2}\right)^2|5A_{SP}+4A_{DP}|^2\right.$$
$$\left.+12\frac{1+8\eta^2+\eta^4}{(1+\eta^2)^2}|A_{DF}|^2\right]. \tag{A7}$$

APPENDIX B: (1+2)-PHOTON DETACHMENT

In this appendix, we prove that for systems without bound states other than the ground state, in the plane-wave approximation and in the perturbation theory regime, angular distributions preserve the fourfold symmetry in the elliptical polarization case. In order to discuss a case from which the generalization to N photons is straightforward, we consider two excess photons. We also consider photon energy such that one photon detachment is allowed, which does not mean that this procedure is not applicable for more general situations. The crucial point is that there are no sums over discrete states, since they are absent, but only integrals containing Dirac delta functions.

In this case, generalization of Eq. (3) is written as

$$M^{(1+2)}_{fg}=\lim_{(\epsilon_1,\epsilon_2)\to0}\sum_{\nu_1\nu_2}\frac{\langle f|\mathbf{D}\hat{\mathbf{e}}|\nu_2\rangle\langle\nu_2|\mathbf{D}\hat{\mathbf{e}}|\nu_1\rangle\langle\nu_1|\mathbf{D}\hat{\mathbf{e}}|g\rangle}{(\omega_g+2\omega_L-\omega_{\nu_2}+i\epsilon_2)(\omega_g+\omega_L-\omega_{\nu_1}+i\epsilon_1)}. \tag{B1}$$

Now the poles are at the positions $k_1^2/2=\omega_1=\omega_g+\omega_L$, $k_2^2/2=\omega_2=\omega_g+2\omega_L$.

When one-photon ionization is allowed using the well-known identity

$$\lim_{\epsilon\to 0}\frac{1}{x+i\epsilon}=\mathrm{P}\left(\frac{1}{x}\right)-i\pi\delta(x), \tag{B2}$$

relation (B1) is written as

$$\begin{aligned}M_{fg}^{(1+2)}=&\mathrm{P}\sum_{\nu_1\nu_2}\frac{\langle k_f|\mathbf{D}\hat{\mathbf{e}}\nu_2\rangle\langle\nu_2|\mathbf{D}\hat{\mathbf{e}}|\nu_1\rangle\langle\nu_1|\mathbf{D}\hat{\mathbf{e}}|g\rangle}{(\omega_1-\omega_{\nu_1})(yh\omega_2-\omega_{\nu_2})}\\&-\pi^2\langle\mathbf{k}_f|\mathbf{D}\hat{\mathbf{e}}|\mathbf{k}_2\langle\mathbf{k}_2|\mathbf{D}\hat{\mathbf{e}}|\mathbf{k}_1\rangle\langle\mathbf{k}_1|\mathbf{D}\hat{\mathbf{e}}|g\rangle\\&-i\pi\langle k_f|\mathbf{D}\hat{\mathbf{e}}|\mathbf{k}_2\rangle\mathrm{P}\sum_{\nu_1}\frac{\langle\mathbf{k}_2|\mathbf{D}\hat{\mathbf{e}}|\nu_1\rangle\langle\nu_1|\mathbf{D}\hat{\mathbf{e}}|g\rangle}{\omega_1-\omega_{\nu_1}}\\&-i\pi\langle k_1|\mathbf{D}\hat{\mathbf{e}}|g\mathrm{P}\sum\frac{\langle k_f|\mathbf{D}\hat{\mathbf{e}}|\mathbf{k}_2\rangle\langle\mathbf{k}_2|\mathbf{D}\hat{\mathbf{e}}|\mathbf{k}_1\rangle}{\omega_2-\omega_{k_2}}.\end{aligned} \tag{B3}$$

Here P denotes the principal value of the corresponding integrals. In the plane-wave approximation, we represent the continuum wave functions as

$$|\mathbf{k}\rangle=\frac{1}{(2\pi)^{3/2}}e^{i\mathbf{k}\cdot\mathbf{r}}. \tag{B4}$$

Using the velocity gauge, it can be shown easily that the dipole matrix element between two continuum states leads to the Dirac delta function, namely,

$$\langle\mathbf{k}|\mathbf{D}\hat{\mathbf{e}}|\mathbf{q}\rangle=\mathbf{k}\hat{\mathbf{e}}\delta(\mathbf{k}-\mathbf{q}). \tag{B5}$$

Thus from the above relation we have

$$\langle\mathbf{k}_f|\mathbf{D}\hat{\mathbf{e}}|\mathbf{k}_2\rangle=\mathbf{k}_f\hat{\mathbf{e}}\delta(\mathbf{k}_f-\mathbf{k}_2)=0 \tag{B6}$$

since $k_f^2/2m=\omega_g+3\omega_L$ and $k_f-k_2=2m\omega_L/(k_f+k_1)\neq 0$.

Finally we have

$$\langle\mathbf{k}_f|\mathbf{D}\hat{\mathbf{e}}|\mathbf{k}_2\rangle=0, \tag{B7}$$

$$\langle\mathbf{k}_f|\mathbf{D}\hat{\mathbf{e}}|\mathbf{k}_2\rangle\langle\mathbf{k}_2|\mathbf{D}\hat{\mathbf{e}}|\mathbf{k}_1\rangle=(\mathbf{e}\cdot\mathbf{k}_f)^2\delta(\mathbf{k}_f-\mathbf{k}_2)\,\delta(\mathbf{k}_2-\mathbf{k}_1)31. \tag{B8}$$

The sum integral

$$\mathrm{P}\sum\frac{\langle\mathbf{k}_f|\mathbf{D}\hat{\mathbf{e}}|\mathbf{k}_2\rangle\langle\mathbf{k}_2|\mathbf{D}\hat{\mathbf{e}}|\mathbf{k}_1\rangle}{\omega_2-\omega_{k_2}} \tag{B9}$$

can be separated into a sum over bound states and an integral that contains only the continuum. The integral vanishes because of Eq. (B6) and only the sum over the intermediate bound states remains. This sum makes the amplitudes of Eq. (14) complex and therefore reduces the fourfold symmetry of angular distributions to twofold symmetry. Under the assumption that the negative ion has no intermediate bound states, the final expression is

$$M_{fg}^{(1+2)}=\mathrm{P}\int d^3k_2d^3k_1\,\frac{\langle k_f|\mathbf{D}\hat{\mathbf{e}}|k_2\rangle\langle k_2|\mathbf{D}\hat{\mathbf{e}}|k_1\rangle\langle k_1|\mathbf{D}\hat{\mathbf{e}}|g\rangle}{(\omega_1-\omega_{k_1})(\omega_2-\omega_{k_2})}. \tag{B10}$$

Since the matrix elements are delta functions, it is easy to calculate the integral and therefore we have

$$M_{fg}^{(1+2)}=\frac{(\hat{\mathbf{e}}\cdot\mathbf{k}_f)^2}{2!\,\omega_L^2}\langle k_f|\hat{\mathbf{e}}\mathbf{D}|g\rangle. \tag{B11}$$

If we use the relations

$$\langle k_f|\hat{\mathbf{e}}\mathbf{D}|g\rangle=\hat{\mathbf{e}}\cdot\mathbf{k}_f\Phi_g(\mathbf{k}_f),$$

$$\hat{\mathbf{e}}\cdot\mathbf{k}_f=k_f\sin\theta\frac{\cos\phi+i\eta\sin\phi}{\sqrt{1+\eta^2}},\quad k_f^2/2=\omega_g+3\omega_L, \tag{B12}$$

we obtain for the angular distributions the formula

$$|M_{fg}^{(1+2)}|^2=\frac{(\omega_g+3\omega_L)^3}{(2^3 2!)^2(1+\eta^2)^3\omega_L^4}|\Phi_g(\mathbf{k}_f)|^2\sin^6\theta(\cos^2\phi+\eta^2\sin^2\phi)^3 \tag{B13}$$

where $\Phi_g(\mathbf{k})$ is the Fourier transform of the ground state. From the above formula, the fourfold symmetry of the PAD for elliptic polarization is evident. Under the same assumptions, it is possible to generalize the above formula to N-photon ionization, with the result

$$\begin{aligned}|M_{fg}^{(N)}|^2=&\frac{(\omega_g+N\omega_L)^N}{(2^N(N-1)!)^2(1+\eta^2)^N\omega_L^{2(N-1)}}\\&\times|\Phi_g(\mathbf{k}_f)|^2\sin^{2N}\theta_f(\cos^2\phi_f+\eta^2\sin^2\phi_f)^N.\end{aligned} \tag{B14}$$

[1] Xin Miao Zhao *et al.*, Phys. Rev. Lett. **78**, 1656 (1997).

[2] C. Blondel and C. Delsart, Laser Phys. **3**, 3 (1993).

[3] C. Blondel and C. Delsart, Nucl. Instrum. Methods Phys. Res. B **79**, 156 (1993).

[4] F. Dulieu, C. Blondel, and C. Delsart, J. Phys. B **28**, 3861 (1995).

[5] M. Bashkansky, P. H. Bucksbaum, and D. W. Schumacher, Phys. Rev. Lett. **60**, 2458 (1988).

[6] P. Lambropoulos and X. Tang, Phys. Rev. Lett. **61**, 2506 (1988).

[7] H. G. Muller, G. Petite, and P. Agostini, Phys. Rev. Lett. **61**, 2507 (1988).

[8] D. Proulx and R. Shakeshaft, Phys. Rev. A **46**, R2221 (1992).

[9] D. Proulx and R. Shakeshaft, Phys. Rev. A **49**, 1208 (1994).

[10] C.-R. Liu, B. Gao, and A. F. Starace, Phys. Rev. A **46**, 5985 (1992).
[11] X. Tang and T. N. Chang, Phys. Rev. A **44**, 232 (1991).
[12] X. Tang *et al.*, Phys. Rev. A **41**, 5265 (1990).
[13] I. Sanchez, F. Martin, and H. Bachau, J. Phys. B **28**, 2863 (1995).
[14] T. N. Chang and Ronq-qi Wang, Phys. Rev. A **43**, 1218 (1991).
[15] H. W. van der Hart, Phys. Rev. A **50**, 2508 (1994).
[16] J. Zhang and P. Lambropoulos, J. Phys. B **28**, L101 (1995).
[17] J. Zhang and P. Lambropoulos, J. Nonlinear Opt. Mat. **4**, 633, (1995).
[18] J. Zhang and P. Lambropoulos, Phys. Rev. Lett. **77**, 2186 (1996).
[19] E. Cormier and P. Lambropoulos, J. Phys. B **29**, 1667 (1996).
[20] J. Sapirstein and W. R. Johnson, J. Phys. B **29**, 5213 (1996).
[21] W. R. Johnson, S. A. Blundell, and J. Sapirstein, Phys. Rev. A **37**, 307 (1988).
[22] E. Cormier and P. Lambropoulos, J. Phys. B **28**, 5043 (1995).
[23] M. L. Goldberger and K. M. Watson, *Collision Theory* (Wiley, New York, 1964).
[24] T. N. Chang and X. Tang, Phys. Rev. A **46**, R2209 (1992).
[25] T. N. Chang, in *Many-body Theory of Atomic Structure*, edited by T. N. Chang (World Scientific, Singapore, 1993).
[26] T. N. Chang and Y. S. Kim, Phys. Rev. A **34**, 2609 (1986).
[27] C. L. Pekeris, Phys. Rev. **126**, 1470 (1962).
[28] P. Lambropoulos, Adv. At. Mol. Phys. **12**, 87 (1976).
[29] M. Crance, J. Phys. B **21**, 3559 (1988).
[30] P. Lambropoulos, Phys. Rev. Lett. **28**, 585 (1972).
[31] R. D. Cowan, *The Theory of Atomic Structure and Spectra* (University of California Press, Los Angeles, 1981).